Available online at www.sciencedirect.com
SCIENCE DIRECT®
International Journal of Heat and Mass Transfer 47 (2004) 4953–4966
International Journal of HEAT and MASS TRANSFER
www.elsevier.com/locate/ijhmt

Optimal shape profiles for cooling fins of high and low conductivity

Florin Bobaru *, Srinivas Rachakonda

Department of Engineering Mechanics, University of Nebraska-Lincoln, Lincoln, NE 68516, USA

Received 20 January 2004; received in revised form 25 June 2004
Available online 20 August 2004

Abstract

We present a numerical approach able to capture the dependence of the optimal shape profiles of thermal fins on the conductivity parameters. We consider the two-dimensional cross-section of a periodic array of fins and involve the third dimension via the thermal boundary layer. The highly conductive fins converge to ''sharp-pointed'', narrow base shapes while the low conductivity ones prefer blunted, wide base fins. The optimal shapes we obtain are similar to the shapes of intestinal villi and stegosaurus plates. A meshfree method, coupled with a gradient-based optimization algorithm, is used to handle the significant shape changes from a simple, generic initial guess to the final, optimal shape. We reach the optimal shapes without remeshing.

Keywords: Non-linear heat-transfer; Shape optimization; Meshfree methods; Thermal fins; Boundary layer; Intestinal villi; Dinosaur cooling fins

1. Introduction and paper organization

Optimal heat-sinks are very important from a technology point of view (see e.g. [1–3]). The cooling fins that from heat-sinks were traditionally studied for mechanical engineering systems but in the past decades with the advent of the computer industry, heat-sinks have found many applications in the microprocessor design (see e.g. [4]).

Using simplifying assumptions and, in many instances, reductions to one-dimensional models, analytical results can be obtained for optimal configurations of thermal fins (see e.g. [5–8]). For more complex cases, two- or three-dimensional heat flow, general boundary conditions, etc. one must rely on numerical methods for finding optimal solutions for thermal fins (see e.g. [9] where the FEM is used). The problem of automatically generating optimal shapes starting from a ''generic'' or simple shape has been, however, problematic.

One difficulty faced by numerical methods such as the finite element method (FEM) is caused by the need of remeshing when the mesh becomes too distorted. Large shape changes are possible when trying to find an optimal shape of an array of cooling fins. With the FEM, one has to employ arduous remeshing every time a large shape change is attempted as a possible improved shape design. This is the case for the material derivative

* Corresponding author. Tel.: +1 402 472 8348; fax: +1 402 472 8292.
E-mail address: fbobaru2@unl.edu (F. Bobaru).

0017-9310/$ - see front matter © 2004 Elsevier Ltd. All rights reserved.
doi:10.1016/j.ijheatmasstransfer.2004.06.013

Nomenclature

A_{max}	maximum cross-sectional area of a fin, m^2
g	gravitational acceleration, m/s^2
Gr	Grashof number
h	heat transfer coefficient $W/(m^2K)$
L_{fin}	length of the fin, m
q	heat flux density, W/m^2
Pr	Prandtl number
Z	height of the fin, m

Greek symbols

β	coefficient of thermal expansion, K^{-1}
δ	boundary layer thickness, m
κ	thermal conductivity, $W m^{-1} K^{-1}$
θ	temperature over the cross-section
θ_∞	ambient temperature
θ_f	average film temperature
ν	kinematic viscosity, m^2/s

method in shape optimization (see e.g. [10, p. 190], [11, p. 109]). An alternative to the moving mesh in the material derivative method is to use the fictitious domain method which solves the shape optimization problem over a fixed FEM mesh. A problem, however, arises as the objective function or the constraints may loose differentiability in this situation (see [11, p. 188]) and convergence of gradient-based optimizers can be compromised.

A different approach to be used instead of the FEM for shape optimization is presented by the newly developed meshfree methods (for review articles on meshfree methods see e.g. [12,13]). Using these methods in the context of the material derivative method for shape optimization, remeshing is not necessary even if the discretization grid gets distorted. A meshfree method has recently been used for optimal shape design of elastic and thermoelastic solids in [14–17], and the results are very encouraging. One case in which large shape changes—from a simple, generic geometry initial design to the optimal design—are involved is that of systems governed by conduction–diffusion equations. The optimal shape design of thermal cooling fins or of mass-diffusion systems provides just two such examples.

Finned surfaces represent one of the most efficient ways of enhancing heat or mass transfer from a surface. The most common geometry used for increasing the surface area is the rectangular cross-section. Triangular, parabolic or cylindrical cross-sectional shapes (see [18, Chapter 8]) are also used in automobile radiators, home heating radiators, semiconductor chip packages, etc. The fin effectiveness (the ratio of heat removed with the fin to heat removed in the absence of the fin) and efficiency (heat removed by the real fin versus heat removed by a perfectly conductive fin) are influenced by the convection and conductivity properties. As the conduction resistance goes to zero, the fin efficiency approaches one (a perfect fin), while when convection resistance goes to infinity, the fin effectiveness goes to zero.

In this paper we show how the competition between the external and internal resistance to heat transfer *determines* the cross-sectional optimal shape for a fin array. A highly conductive fin in a "not-too-high" convective conditions prefers to extend the material away from the base in the form of thin and sharp-pointed fins. On the other hand, a less conductive fin in the same convective ambient tends to avoid developing sharp shapes that cool to fast and therefore reduce the heat transfer. These fins are expected to show round-ended fins with wide bases as their optimal cross-sectional configuration.

We provide a scheme for automatically determining the optimal shape of a conduction–diffusion system. We start from a shape that is very different from the final, optimal configuration. We employ a meshfree method and large shape changes are dealt with without remeshing. We show that a general formulation based on the meshfree solution of the non-linear heat-transfer equations coupled with a gradient-based optimization scheme is effective in determining important characteristics and details of the optimal shapes for *varying conductivity parameters*. The context of this work is that of laminar flow under natural convection. Other types of conditions can be considered using the current development.

The main contributions of this paper are:

1. We develop a *2 and 1/2*-dimensional numerical scheme based on a meshfree method capable of capturing the *dependence of the optimal shape on conductivity* parameters for optimal shape design of cooling fins;
2. We establish a connection between optimal shapes of thermal systems and those of biological systems participating in mass diffusion or heat transfer, such as intestinal villi or dinosaur cooling plates.

The paper is organized as follows: in Section 2 we review previous work. In Section 3 we give the description of the problem, the optimization setup and the meshfree solution of the non-linear heat transfer problem with a convection boundary that is designable. In Section 4 we discuss the similarity between the mass and heat

transfer systems and present numerical results for high and low conductivity parameters. Future work and conclusions are gathered in Section 5.

2. Previous work

In this section we note some optimal shapes observed in, or inspired by, natural systems. The motivation for generating optimal shapes from simple, generic configurations can be drawn from the immense variability of forms in nature. We also review works on optimal shape design of thermal fins.

2.1. Optimal shapes in nature

The enormous variety of shapes present in natural systems may be attributed to the multitude of local/global minimizers that exist. With a proper mathematical description of the underlying physical/chemical/biological processes coordinating the state of a natural system, one can follow an optimization scheme similar to the one described in this paper and be able to reproduce the naturally occurring shapes.

One way for increasing heat or mass transfer between two systems is to increase the surface area that participates in the transfer. Many technological applications use extended surfaces for that purpose. Thermal cooling fins represent just one such example. Extended surfaces for enhanced transfer are seen in natural systems also, for instance the intestinal villi. Plates and spines of the Stegosaurus dinosaur functioned, apparently, as temperature regulators (see [19]). The plates formed a scaffolding for the support of a richly vascularized skin that would have acted as an efficient heat exchange structure. These fins would have functioned well as forced convection fins to dissipate heat or as heat absorbers [19]. The particular shape of an extended surface does influence its efficiency and the effectiveness of the entire fin array is affected by the spacing between the periodic fins (see e.g. [18]).

2.2. Thermal fins and meshfree methods for optimal shape design

Finned surfaces in natural convection provide a significant improvement in efficiency (increasing the heat flux) compared to unfinned ones. Both the fin thickness and the spacing between fins are determining factors that cannot be neglected in optimizing the total fin array heat transfer (see e.g. Bar-Cohen [5]). These two factors influence both the efficiency of individual fins and the number of fins that can be accommodated in a given area.

A number of studies have attempted to find the optimal configuration for a vertical fin array. Recently, Bejan and coworkers have introduced the "constructal" theory (see e.g. [7,8,20,21]). Heat flow problems between a volume and one point are treated. The optimal flow structure for minimal global resistance is found to be a tree. The works above-cited use simple geometries of elemental regions in order to build more complex structures. They optimize the size rather than the shape. The selected simple geometries allow for a semi-analytical one-dimensional approach, where solutions are found for the heat-transfer equation with one spatial coordinate. Fractal-like features are thus obtained and their relevance to the properties of natural flow structures are discussed. Earlier studies on searching for the optimal spacing between parallel plates under natural convection cooling can be found in Bar-Cohen [5] and Bar-Cohen and Rohsenow [6]. In these works, a restricted one-dimensional model for heat transfer is used for plates of rectangular cross-section only. The optimal spacing between efficient isothermal fins is found in [6]. In [5] the case studied is that of fins whose temperature varies with distance from the base. It is found that the optimum fin width and spacing depend upon the fin thickness and its thermal conductivity. Optimum design of heat-sinks for electronic applications are discussed in, for example, [3]. Fin flow, the number of fins, fin length and height are allowed to vary.

In shape optimization problems where the initial shape changes drastically to reach the final, optimal shape, the need of remeshing is crucial in a solution process that used the FEM or BEM as analysis tools. In any remeshing algorithm, the transfer of data from the old mesh to the new mesh incurs errors. We would benefit from using an analysis tool that avoids remeshing even when large shape changes are needed in the shape optimization process.

Meshfree methods have been proposed that overcome the remeshing problems. The element-free Galerkin (EFG) method [22] is a meshfree method which has been recently employed in shape optimization problems of elastic and thermoelastic solids by Bobaru and Mukherjee (see [16]). Shape sensitivities of elastic solids with the EFG methods have been addressed in Ref. [15] and for thermoelasticity in Bobaru's thesis [14]. In [16], the problem of optimizing an initially triangular-shaped thermal fin for increased heat-flux through the base of the fin under area constraints, has produced strikingly different (and better) results than previous FEM-based analysis (see Hou and Sheen [9]) of the same problem. The main result obtained in [16] is the automatic subdivision of the original fin into sub-fins in search for a optimal shape. There is no need for remeshing, even if large shape changes take place from on iteration to the next.

A study of the influence of the number of design variables selected in the problem's solution was performed in [16]. It appeared that the more design variables were

chosen to describe the shape of the designable boundary, the more sub-fins would result at the end of the optimization process. The objective function was improved with the increase of the number of sub-fins developed. The increase in the surface area that was exposed to the cooling ambient implied an increase in the objective function value.

2.3. The thermal boundary layer and optimal shape design

The study in [17] answered the following questions: "Is there a limiting value on the number of sub-fins generation in maximizing the heat flux through the base of the fin structure? How close can the sub-fins get to one another and still release heat efficiently? What is the optimal number of fins, the optimal shape and the optimal spacing between them from maximum heat flux?" Previous results obtained in [16] indicated that the "optimal" fin structure is one with an infinite number of fins of infinitesimal thickness closely packed together. That would mean that the problem is ill-posed: there exists no solution. In [17], the above ill-posed problem is elucidated. We noticed that non-existence of optimal solutions is eliminated if we considered the thermal boundary layer that forms in the ambient medium along the fin surface. The problem was regularized by requiring no overlap of the boundary layer.

The optimal shape design of cooling fins studied in [16] and [9] considered the 2D cross-section of a triangular thermal fin. In Sections 3.1 and 3.2 of this paper we present the approach that regularizes the ill-posed problem (see also [17]). We select a unit-cell from a three-dimensional fin and focus in optimizing the shape of the cross-section. The use of the third dimension is critical in regularizing the problem since we use a enforce no overlap for the thermal boundary layer that forms at the fin's surface. The details of evaluating the violation of the boundary layer overlap constraint are given in [17]. The third dimension is involved since the height of the fin array determines the thickness of the boundary layer. Moreover, the height of the fin determines if the natural convection conditions give rise to laminar or turbulent flow. We select the fin's height such that the resulting flow along the entire height of the fin is laminar. In [17], a new and very efficient algorithm for eliminating the overlap at the top cross-section of the fin array has been introduced. The algorithm works for the case in which the boundary is given by a function.

3. Problem description

We consider an array of vertical (z-direction), periodic fins. The "base" of the fin ($y = 0$ plane in Fig. 1(a)) is attached to a system with a constant temperature $\theta_0 = 500$ K. The fin array is exposed to an ambient temperature of $\theta_\infty = 300$ K. We assume natural convection and the height of the fin is selected so that the flow is laminar over the entire height of the fin. The goal is to find the optimal shape of the cross-section of the fin array that results in maximum heat-transfer through its base. Naturally, a volume constraint has to be imposed if the problem is to be well-posed. One can notice that if the fins are widely spaced or almost isolated, the heat transfer rates are high but the total area exposed to the ambient is low and this results in a low total heat transfer for the entire fin array. If the fins are, on the other hand, closely packed together, total fin area is high but heat flux is low because of the thermal boundary layer interaction between individual fins (the fins are exposed to each other instead of being exposed to the ambient temperature). An optimal spacing between the individual fins, as well as the shape profile of the fins is sought at the end of the optimization scheme.

The search for the optimal shape starts with a generic, unfinned construct. The cross-section of a unit-cell for such a system is rectangular (see Fig. 1(b)). The

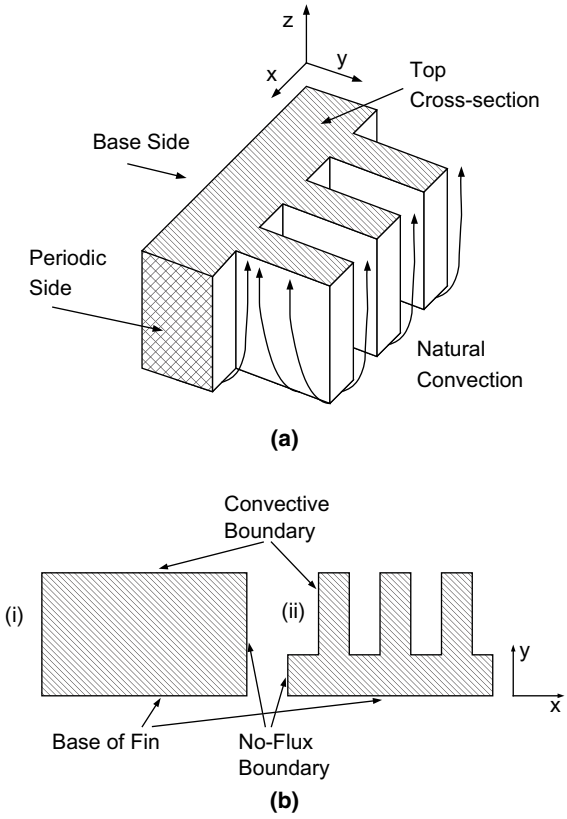

Fig. 1. The geometry of a thermal fin. (a) A three-dimensional cooling fin array under natural convection conditions. The base side in the back is attached to a system at constant temperature. (b) Unfinned (i) and finned with rectangular fins (ii) top cross-sections of a cooling system.

optimization problem is to find the best shape of the cross-section that maximizes heat-flux while the cross-sectional area is constrained to be less than an arbitrarily selected value of 60% of the original rectangular area.

Using the heat-transfer equation alone in determining the optimal shape, leads to non-existence of solutions since we cannot account for the heating of the ambient in the boundary layer around each fin. As a result, the "optimum" will be an infinite number of fins, infinitely thin and closely packed together. As we have recently shown (see [17]), in order to make the problem well-posed an additional constraint has to be added to the optimization problem. The constraint adopted in [17] was to impose no boundary layer overlap. A different constraint is mentioned by Haslinger and Mäkinen (see [11, pp. 10–12]) which suggest constraining the length of the convective boundary curve (see Fig. 1(b)). Such a constraint, however, seems artificial. In fact, determining the optimal length of the boundary is part of the problem here. The boundary layer overlap constraint that we use regularizes the ill-posed problem [23] in the sense that it eliminates non-existence of solutions.

The focus of this paper is to apply the shape optimization scheme for materials with different conductivity parameters and notice the effect, if any, on the optimal shape. To this end, we consider the optimization of the two-dimensional cross-section of the fin array by including the thickness of the boundary-layer constraint at the top of the fin. We work with a unit cell for a periodic array of fins. The length of such unit cell fin has been determined in [17]. Periodic boundary conditions on the two sides of the fin imply no heat-flux through these boundaries (see Fig. 1(b)).

3.1. The shape optimization setup and the boundary layer constraint

The objective function in the optimal shape design problem is the heat-flux density through the base, while the constraints are imposed on the cross-sectional area and the boundary layer overlap, as follows:

$$\begin{aligned}
&\text{minimize} && F(y_1,\ldots,y_p) = -\frac{\int_{\Gamma_\theta^0} q\,\mathrm{d}\Gamma}{L_{\text{fin}}} \\
&&& (\equiv \text{ maximize heat} - \text{flux density}) \\
&\text{area constraint} && H_1(y_1,\ldots,y_p,\mathbf{x}) = 1 - \frac{\int_\Omega \mathrm{d}\Omega}{A_{\max}} \geqslant 0, \\
&\text{overlap constraint} && H_2(y_1,\ldots,y_p,\mathbf{x}) = 1 - \frac{v}{v_{\max}} \geqslant 0, \\
&\text{simple bounds} && \mathbf{l} \leqslant \mathbf{y} = [y_1,\ldots,y_p] \leqslant \mathbf{u}.
\end{aligned} \tag{1}$$

Here, L_{fin} is the length of the design boundary and the design variables $y_1,\ldots,y_p$ are the y-coordinates of some of some grid nodes on the design boundary Γ_θ^2. The shape of the design boundary is determined by these design variables (control points). We require the rest of the discretization nodes on Γ_θ^2 to change their positions so that they are on the spline function interpolating the design variables $y_1,\ldots,y_p$. We use a shape preserving spline, namely the Akima spline (see [24]) for the boundary interpolation through the control (design) points. Also, v is the "amount of overlap" and $v_{\max}$ a small positive number that represents a maximum allowed overlap. This is chosen to improve convergence and accept shapes that produce a negligible boundary layer overlap. In our calculations we take $v_{\max} = 0.05L_{\text{fin}}$ which is 5% of the total length of the unit-cell base.

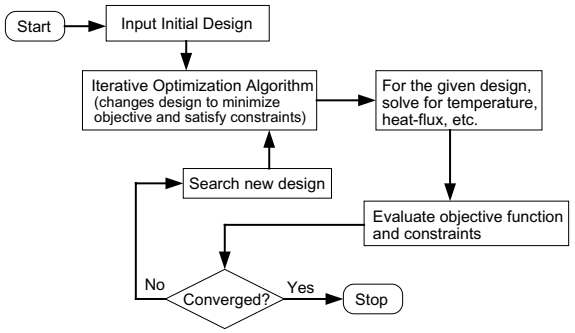

Fig. 2. The flowchart for the optimization algorithm. A meshfree method (EFG) is used in solving for temperatures, heat-flux, and the boundary layer-thickness. Large shape changes during the optimization search do not require remeshing in the EFG method.

We use a sequential quadratic algorithm implemented in the IMSL numerical library (DNCONF) to solve the optimization problem above [25–27]. The optimizer uses the values of the objective function and constraints every time a new set of the design variables is selected and during the line search. The iterative optimization process follows the diagram depicted in Fig. 2. Shape sensitivities (see, e.g. [28]) are calculated internally by the optimizer using finite differences approximations in an adaptive way (see [25]). The selection of finite difference gradients (sensitivities) is motivated here by simplicity rather than efficiency. Results on accurate and efficient schemes for shape sensitivities calculations using meshfree methods can be found in, for example, [15].

We next present a way of evaluating the boundary layer overlap v and the objective function F in problem (1) at each optimization iteration.

3.2. The meshfree solution for the non-linear heat-transfer equations

During the iterations of the gradient-based optimizer we are required to provide means for calculating the value of the objective function and constraints. The

temperature and heat-flux are determined by solving the non-linear heat-transfer equation (2) below over the domain Ω, the top cross-section of the fin (see Fig. 1(b)).

$$\begin{cases} \Delta\theta = 0 & \text{in} \quad \Omega \\ \theta = \theta_0 & \text{on} \quad \Gamma_\theta^0 \\ \kappa\nabla\theta\cdot\mathbf{n} = \bar{q} & \text{on} \quad \Gamma_\theta^1 \\ \kappa\nabla\theta\cdot\mathbf{n} = h(\theta)(\theta-\theta_\infty) & \text{on} \quad \Gamma_\theta^2 \end{cases} \tag{2}$$

This equation is valid for laminar flow in free convection past a vertical wall with constant temperature in the vertical direction. To ensure laminar flow we have to limit the allowable height for the fin. The height of 0.4 m selected in our numerical results gives rise to laminar flow.

The boundary value problem in Eq. (2) is linear except in the boundary condition prescribed over the convective region Γ_θ^2. The heat transfer coefficient is a non-linear function of the temperature on the convective boundary. In terms of the height z of the fin, the heat transfer coefficient is given by (see, e.g. [29]):

$$h(z) = \frac{2\kappa Pr^{1/2}}{z[336(Pr+5/9)]^{1/4}} Gr_z^{1/4}. \tag{3}$$

The heat transfer coefficient depends on Grashof's number which implies a dependence on the fin's temperature on Γ_θ^2, since

$$Gr = \frac{g\beta(\theta-\theta_\infty)z^3}{\nu^2}. \tag{4}$$

The dependency of h on $\theta_{|\Gamma_\theta^2}$ is more complicated than the root-four behavior apparent from Eqs. (3) and (4). That is because Prandtl number and the convective factor $g\beta/\nu^2$ in Grashof's number also vary with the temperature θ on Γ_θ^2 (see Table 1 in [17] or the appendix in [29]). The values we use for the ambient are those of air at one atmosphere and for the range of temperatures and conditions specified above. The ambient fluid properties are captured by the "convective term" $g\beta/\nu^2$. These properties are normally evaluated at the film "average" temperature $\theta_f = (\theta_w + \theta_\infty)$ (see [29, p. 298]) where θ_w is the "wall" temperature, i.e. the temperature of the fin's convective boundary.

We solve this non-linear problem using a "fixed-point" type iterative scheme. Assume that at iteration k we have solved for the temperature field θ_k over the cross-section of the fin. The solution for the temperature field θ_{k+1} at the next iteration is then given by the solution to the following *linear* boundary value problem:

$$\begin{cases} \Delta\theta_{k+1} = 0 & \text{in} \quad \Omega \\ \theta_{k+1} = \theta_0 & \text{on} \quad \Gamma_\theta^0 \\ \kappa\nabla\theta_{k+1}\cdot\mathbf{n} = \bar{q} & \text{on} \quad \Gamma_\theta^1 \\ \kappa\nabla\theta_{k+1}\cdot\mathbf{n} = h(\theta_k)(\theta_{k+1}-\theta_\infty) & \text{on} \quad \Gamma_\theta^2 \end{cases} \tag{5}$$

The iterations continue until $\|\theta_{k+1}-\theta_k\| < \epsilon$, with epsilon a preset tolerance. This process amounts to solving a set of linear systems that are formed by discretizing the weak forms corresponding to the Eq. (5):

$$\int_\Omega \kappa\nabla\theta_{k+1}\cdot\nabla\eta\,d\Omega - \int_{\Gamma_\theta^1}\bar{q}\eta\,d\Gamma + \int_{\Gamma_\theta^2} h(\theta_k)\theta_{k+1}\eta\,d\Gamma - \int_{\Gamma_\theta^2} h(\theta_k)\theta_\infty\eta\,d\Gamma = 0 \quad \text{for any } \eta\in V, \tag{6}$$

where $\eta \in V = \{\eta \in H^1(\Omega), \eta = 0 \text{ on } \Gamma_\theta^0 \text{ in the sense of trace}\}$ are the test functions.

The element-free Galerkin (EFG) discretization of Eq. (6) leads to the following linear system of equations:

$$\mathbf{M}(\theta_k)\boldsymbol{\theta}_{k+1} = \mathbf{f}(\theta_k), \tag{7}$$

where the global matrix $\mathbf{M}(\theta_k)$ and the right-hand side vector $\mathbf{f}(\theta_k)$ are defined as:

$$\mathbf{M}(\theta_k) = \int_\Omega \kappa\boldsymbol{\Lambda}^{-1}\mathbf{B}^T\mathbf{B}\boldsymbol{\Lambda}^{-T}\,d\Omega + \int_{\Gamma_\theta^2} h(\theta_k)(\boldsymbol{\Lambda}^{-1}\boldsymbol{\phi})\otimes(\boldsymbol{\Lambda}^{-1}\boldsymbol{\phi})\,d\Gamma \tag{8}$$

$$\mathbf{f}(\theta_k) = \int_\Omega Q\boldsymbol{\Lambda}^{-1}\boldsymbol{\phi}\,d\Omega + \int_{\Gamma_\theta^1}\bar{q}\boldsymbol{\Lambda}^{-1}\boldsymbol{\phi}\,d\Gamma + \int_{\Gamma_\theta^2} h(\theta_k)\theta_\infty\boldsymbol{\Lambda}^{-1}\boldsymbol{\phi}\,d\Gamma \tag{9}$$

The symbol $\otimes$ above stands for the exterior (tensor) product. The matrix $\boldsymbol{B}$ above is used to approximate the gradient in the N-dimensional discretization space as $\nabla\theta^{(N)} = \mathbf{B}\hat{\boldsymbol{\theta}}$ and is given by:

$$\mathbf{B} = \begin{bmatrix} \frac{\partial\phi_1}{\partial\mathbf{x}_1} & \cdots & \frac{\partial\phi_N}{\partial\mathbf{x}_1} \\ \frac{\partial\phi_1}{\partial\mathbf{x}_2} & \cdots & \frac{\partial\phi_N}{\partial\mathbf{x}_2} \end{bmatrix}, \quad \text{with} \quad \boldsymbol{\phi} = \begin{bmatrix} \phi_1 \\ \vdots \\ \phi_N \end{bmatrix},$$

$$\boldsymbol{\theta} = \begin{bmatrix} \theta_1 \\ \vdots \\ \theta_N \end{bmatrix}, \tag{10}$$

where ϕ_i are the MLS approximation functions. The matrix $\boldsymbol{\Lambda}$ in (8) is accounting for imposing the essential boundary conditions via a transformation method (see [30]). The transformation of the shape functions is necessary in the EFG method since the shape functions do not satisfy the Kronecker delta property. Other methods for imposing the geometric boundary conditions are available (see a review in [13]). The temperature values the nodes, $\theta_j = \theta(x_j)$, $j = 1,\ldots,N$, are expressed in terms of some "fictitious" temperatures as:

$$\theta_j = \theta(x_j) = \sum_i \phi_i(x_j)\hat{\theta}_i = \sum_i \Lambda_{ij}\hat{\theta}_i = (\boldsymbol{\Lambda}^T\hat{\boldsymbol{\theta}})_j \tag{11}$$

$$\hat{\boldsymbol{\theta}} = \boldsymbol{\Lambda}^{-T}\boldsymbol{\theta}, \quad \hat{\boldsymbol{\eta}} = \boldsymbol{\Lambda}^{-T}\boldsymbol{\eta} \tag{12}$$

where $\hat{\theta}_i$ are the "fictitious" nodal temperature values, and $\Lambda_{ij} = \phi_i(x_j)$ is the transformation matrix.

The solution to the non-linear heat-transfer equation provides the temperature profile across the fin array. The heat-flux through the base can then be calculated, as well at the thickness of the boundary layer given by (see e.g. [29]):

$$\delta = \delta(\theta - \theta_\infty, z) = \left[\frac{336\left(Pr + \frac{5}{9}\right)}{Pr^2}\right]^{\frac{1}{4}} \frac{z}{Gr^{1/4}} \tag{13}$$

The area constraint is easily determined using the location of the design variables and the spline interpolation of the design boundary. For the evaluation of the boundary layer overlap we provide a simple algorithm that estimates the amount of overlap using only the x-coordinates of points on the outer limit of the thermal boundary layer at the top cross-section $z = 0.4$ m (see [17] for details). The efficient algorithm in [17], however, is applicable only when the fin's boundary is given by a function. For the more general case when the boundary is a general curve the algorithm needs modification. This subject is currently under investigation.

4. Optimal shapes for high and low conductivity parameters

We select two types of materials for the thermal fin: high conductivity materials (aluminum and copper) and a relatively low conductivity material which has a high melting point (titanium). We also choose a fictitious material with a conductivity equal to unity (compare that to the conductivity of copper, 389 W/m K at 200 °C, or of titanium of 20 W/m K at 200 °C). Thermal cooling fins are normally made from high conductivity materials to increase their effectiveness, but in high temperature conditions, if cooling fins are required, a highly conductive material might not be usable due to low melting temperature point. The alternative is to use a material that has a high melting point and, in general, these materials have lower conductivity parameters. The unit conductivity material presents a noticeable difference between the temperature at the base of the fin and the temperature at the tip of the fin. In the numerical tests that follow, the relative temperature change across the fin for the optimal shape is less than 0.1% for aluminum and copper, about 1% for titanium, and around 13.5% for the unit-conductivity material.

4.1. Relation to optimal shapes of biological systems in mass transfer problems

An additional reason for considering fins made from low conductivity materials is given by the similarity of heat and mass transfer. Many biological systems use extended surfaces to increase the exchange of heat and/or mass with the environment. The "conductivity" of these systems can be considered to be low compared to that of highly conductive metals like copper or aluminum. For example, intestinal villi are extended surfaces (fins) that enhance the mass transfer of nutrients from the intestine to the blood stream. Possible questions are: "What determines the intestinal villi shape and spacing?" and "Is there any relation between the characteristics of the mass transfer and the shape and spacing of the villi?" The conjecture we state is:

The shape of the intestinal villi is determined, in part, by the mass transfer characteristics: the convection–diffusion through the wall of the villus and mass diffusion through the villus.

The steady-state equations for the incompressible diffusion equation are the same as the non-linear heat-transfer equations give by (2). The well-known analogy is obtained if one operates the following replacements:

temperature θ	$\Longleftrightarrow$	mass density ρ
thermal diffusivity $\kappa/\rho c_p$	$\Longleftrightarrow$	mass diffusivity D
heat transfer coefficient h	$\Longleftrightarrow$	mass transfer coefficient h_m
Prandtl number Pr	$\Longleftrightarrow$	Schmidt number Sc
Nusselt number Nu	$\Longleftrightarrow$	Sherwood number Sh

One can extract information about optimal shape of intestinal villi by studying optimal shape for thermal fins. The analogy thermal fins—villi is limited, however, by the additional biological constraints and requirements that have to be met by a bio-system. For instance, the intestinal villi are not homogeneous and isotropic materials as the cooling fins that we study are.

4.2. Numerical tests and results

A unit-cell for the fin array described in Section 3 has been determined in [17] to have a length of about 0.05 m. We consider a number of design variables selected on the top side of the fin cross-section (the convective boundary in Fig. 1(b)) equal to five. A shape-preserving spline (see [17]) is used to interpolate through these points and define the shape of the unit-cell fin. Increasing the number of shape design variables does not change the shape in any significant way (as long as we use the same type of interpolation functions), and as a result the heat-flux does not change. The boundary layer constraint is critical in determining the unit-cell length for the array of fins. The optimization problem that uses

Table 1
Some material properties for the selected materials

Material	Melting point (K)	Density (at 20 °C) (ρ (kg/m^3))	Thermal conductivity at 200 °C (κ (W/m K))
Pure aluminum	933	2702	238
Pure copper	1356	8933	389
Titanium	1953	4500	20
Unit conductivity	NA	NA	1

an area constraint only, is ill-posed (see [17,31]) as it leads to non-existence of solutions.

Material properties for the aluminum and copper (highly conductive but with low melting points), and titanium and the unit-conductivity material (with low conductivity) are shown in Table 1.

In all subsequent tests we employ a grid of 31×31 nodes. This grid has been determined sufficient to capture with accuracy the temperature profile. The nodes on the grid move in the direction of the width of the fin in search for a better shape. The motion is controlled by the design variables. For details see [17].

The optimal shape design for the thermal system under consideration is sensitive to the initial guess due to the existence of a multitude of local minima. Gradient-based optimization algorithms can get trapped at these local minima. Choosing an evolutionary algorithm instead, such as genetic algorithms or simulated annealing, may present a better chance of achieving the global optimum. The trade-off, however, is a very significant increase in the computational cost. The number of iterations required by evolutionary algorithms to converge is, generally, several orders of magnitude larger than when using gradient-based methods. Here we use gradient-based optimization algorithms and vary the starting guess in order to increase the chances of reaching a global minimizer.

We observed that many of the various perturbations of the flat, unfinned shape lead to poorer or similar local minimizers to the ones obtained from the two starting guesses described below. By using a set of different initial shapes we have no guarantee that we reach the global minimum (within the class functions used here for describing the convective boundary) since there is no analytical result available for this problem. Nevertheless, the results show that one or more constraints are active at the final iteration. This is an indication that we probably are "close" to the best possible shape.

We perform the following tests for each of the four materials selected above:

- The "round guess" (RG): start with the initial shape shown in Fig. 3(a).
- The "sharp guess" (SG): start with the initial shape as in Fig. 3(b).

The starting and final values for the design variables are given in columns 2 and 3 in Table 2. We also include

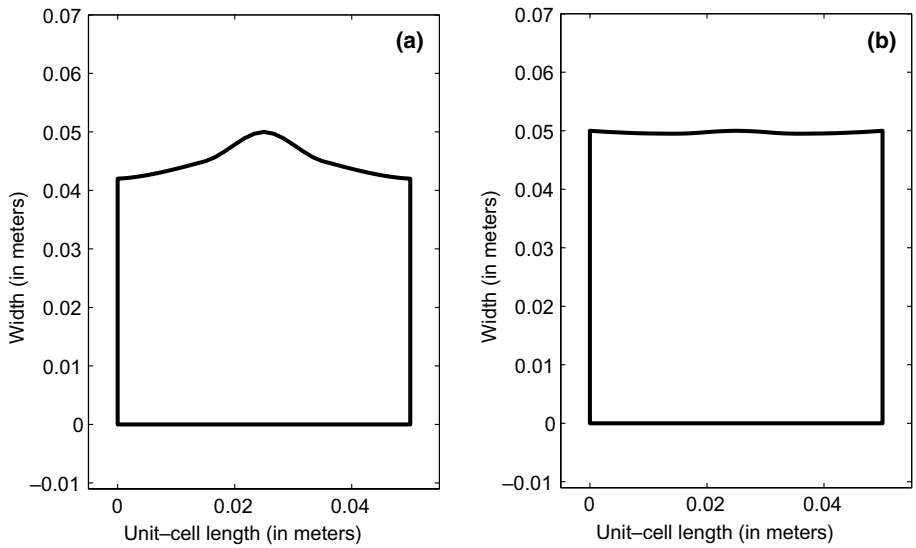

Fig. 3. Two starting guesses. (a) The "round guess" (RG) starting cross-section. (b) The "sharp guess" (SG) starting cross-section.

Table 2
Optimization results for starting guesses RG and SG and the four selected materials

Material and number of iterations	Initial values of DVs[a] (m)		Final values of DVs (m)	Initial value of heat flux (W/m^2)	Final value of heat flux (W/m^2)	Area constraint final value	Boundary layer constraint final value
Al	RG[b]	0.042	0.015				
6 iterations		0.045	0.027	986.06	1661.26	0.73×10^{-1}	0.35×10^{-6}
		0.050	0.050				
Al	SG[c]	0.050	0.050				
12 iterations		0.0495	0.017	925.9	1729.6	0.178	-0.45×10^{-9}
		0.050	0.015				
Cu	RG	0.042	0.015				
7 iterations		0.045	0.027	985.52	1660.64	0.73×10^{-1}	-0.33×10^{-8}
		0.050	0.050				
Cu	SG	0.050	0.050				
19 iterations		0.0495	0.017	923.44	1730.48	0.177	0.466×10^{-1}
		0.050	0.015				
Ti	RG	0.042	0.015				
19 iterations		0.045	0.027	975.46	1637.42	0.73×10^{-1}	0.19×10^{-1}
		0.050	0.050				
Ti	SG	0.050	0.050				
18 iterations		0.0495	0.035	915.8	1314.8	-0.11×10^{-3}	0.14×10^{-1}
		0.050	0.033				
Unit-conductivity	RG	0.042	0.015				
8 iterations		0.045	0.0274	797.6	1280	0.74×10^{-1}	-0.47×10^{-10}
		0.050	0.05				
Unit-conductivity	SG	0.05	0.015				
19 iterations		0.0495	0.0275	745.1	1279	0.72×10^{-1}	0.11
		0.050	0.05				

[a] DVs ≡ design variables.
[b] The "round guess" in Fig. 3(a).
[c] The "sharp guess" in Fig. 3(b).

data about the number of iterations performed by the optimizer until convergence is achieved. Notice that we use five design variables on the designable boundary (the top line in Fig. 3(a) and (b)) but only three values are shown for each case in Table 2. That is because we search for symmetrical shapes, therefore the design variables $d_1,\ldots,d_5$ have to satisfy the conditions: $d_5 = d_1$ and $d_4 = d_2$. The nodes whose coordinates are the design variables are equally spaced along the horizontal direction.

With a round initial guess RG, the final optimal shape for the aluminum fin is shown in Fig. 4. The optimal shapes for copper, titanium, and the unit-conductivity fins are almost the same (see data for final values of design variables in Table 2). At the final iteration, the area constraint is not violated in any of the four materials, and the same is true for the boundary layer constraint with the exception of copper where the value of the violation is insignificant (on the order of 10^{-8}).

The number of iterations required to reach these shapes is remarkably small, in general less than 20 and in many instances less than 10. Methods of shape optimization based on evolutionary algorithms require hundreds of iterations. The efficiency of our method is due,

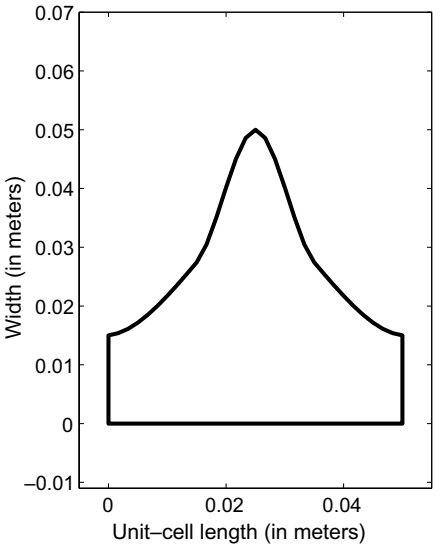

Fig. 4. The optimal shape for aluminum starting with the RG cross-section. The optimal shapes for copper, titanium and the unit-conductivity material are the same (see data for final values of design variables in Table 2).

in part, to the use of a gradient-based optimization algorithm and, perhaps even more so, to the meshfree method of solution that allows large shape changes from one iteration to the next *without remeshing*.

With the "sharp" initial guess SG, the final optimal shape for the aluminum and the unit-conductivity are shown in Fig. 5(a) and (b). This is a striking result. Starting from the *same initial guess*, with only the conductivity parameter being different, the aluminum and the unit-conductivity material fins converge to totally different shapes! The unit-conductivity fin converges almost to the same shape as that given by the RG shape (see Table 2). The optimal fin for copper is identical in shape to that of the aluminum fin, as one can see from Table 2. We note the increase in the objective function value for the aluminum and copper optimal sharp pointed fins compared to the value given by the optimal "round" shape for the same materials. The relative increase is around 4%.

The titanium fin gets trapped in a local minimum shown in Fig. 5(c). The objective function value is significantly lower than the result from the RG for the same

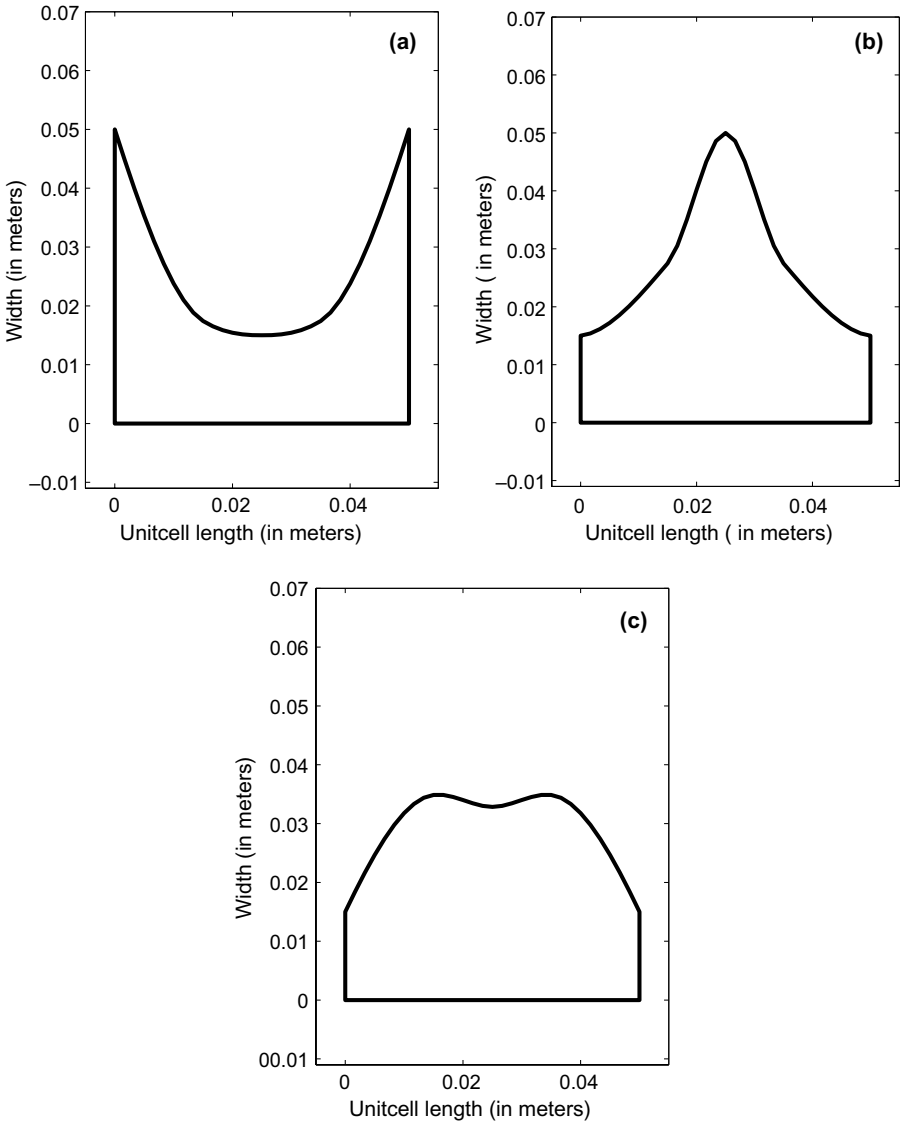

Fig. 5. Final shapes when using the SG shape as the starting guess for the fin cross-section. (a) The optimal shape for aluminum starting with the SG cross-section. (b) The optimal shape for the unit-conductivity material starting with the SG cross-section. (c) A local minimizer for the optimal shape for titanium starting with the SG cross-section. Note that the trend is different from the sharp-pointed optimal shape to which the aluminum fin converges.

material. Moreover, if we place the unit-cell into a periodic array of fins we will generate a large boundary layer overlap at the ends of the each fin. The heat flux for the fin array will be less than the sum from all fins, since overlap of the boundary layer reduces heat-transfer. To get out of the local minimum we could restart from a perturbed shape. We, however, choose a different path that can eliminate the boundary layer overlap for entire fin array. We present this in Section 4.4.

In summary, the round-guess RG leads to a shape that is independent of the conductivity. The SG, however, sends the highly conductive materials to a shape that is better than the one from RG. The low-conductivity material minimum does not change between the RG and the SG and suggests that this shape is the global minimum for low conductivity materials. We explain the above observations as follows: the highly conductive material will prefer shapes that have sharp spikes since these shapes provide large surface areas, and, due to the high conductivity, the boundary temperature along these spikes is high, leading to efficient heat transfer. On the other hand, the low conductivity materials avoid these long and narrow shapes since they would cool fast and large boundary areas will not contribute to efficient heat transfer. We recall that convective heat transfer is proportional to the temperature difference between the boundary of the fin and the ambient temperature (see Eqs. (3) and (4)).

4.3. Connection to shapes of biological systems

These observations offer a possible explanation for the shape of some biological structures. The intestinal villus is round and has a large base because the mass diffusion inside the villus is slow relative to the mass transfer between the ambient fluid and its wall. The round shape is, therefore, the optimal shape that maximizes the mass transfer. A comparison with the transversal cross-section of dinosaur fins [19] can also be made. The cross-section of these fins can be considered sharp pointed and having a narrow base (see [32]). We infer that the conduction of these fins, working under forced convection conditions, was high relative to the heat-transfer rate at the surface of the fin. The fins evolved in this "sharp-pointed" cross-section in order to maximize the heat-transfer under the given conditions.

4.4. Eliminating the boundary layer overlap for the periodic fin array

Using the periodic boundary conditions, the fin array for aluminum looks as in Fig. 6(a) when the initial guess

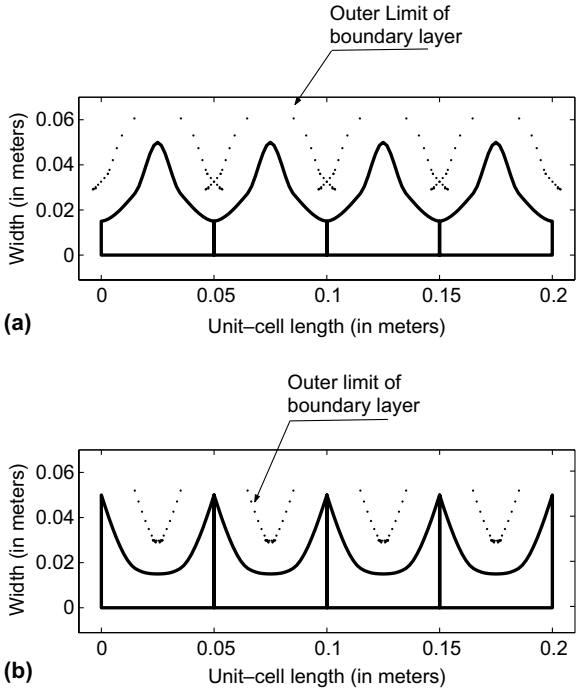

Fig. 6. Using the periodic boundary conditions for constructing the fin array. (a) The periodic array of fins for aluminum with the RG shape as the initial guess. Notice the overlap of the boundary layer. (b) The periodic array of fins for aluminum with the SG shape as the initial guess.

is the RG shape, and as in Fig. 6(b) when we start with the SG shape.

The periodic fin shows overlap of the boundary layer for the round guess case (see Fig. 6(a)). The values obtained for the objective function in these cases are larger than the actual, true values. In order to avoid the overlap in these cases, we can impose an additional constraint that requires the slope at the end points to be zero.

$$\left.\frac{\mathrm{d}f(x)}{\mathrm{d}x}\right|_{x=a} = 0, \quad \text{and} \quad \left.\frac{\mathrm{d}f(x)}{\mathrm{d}x}\right|_{x=b} = 0$$

where f is the function that describes the boundary of the fin, and $x = a$, $x = b$ are the ends of the fin in the horizontal direction. Numerically, this is accomplished by imposing the two left-most and two right-most discretization nodes on the boundary, have the same y-coordinates (along the fin's width direction), respectively.

The results for the constrained slope at the ends of the unit fin are summarized in Table 3 for aluminum and the unit-conductivity material. The optimal shape for aluminum is given in Fig. 7. Note that the optimal shape for the unit-conductivity material is nearly the same as for aluminum. The boundary constraint violation is negligible and is in the order of 10^{-3} for an individual fin. For aluminum, the relative change in heat-flux between the "optimal" round shape (obtained using the additional geometrical constraint) and the sharp fin construct is significant: 11.3%.

The optimal shape for the titanium and the unit-conductivity fins starting from the guess that leads to sharp-pointed fins in the highly conductive case is the same as the one in Fig. 7. The low-conductivity fins prefer shapes with convex tips.

4.5. Shape dependence on the conductivity parameters

We notice that starting from the same guess SG, the high conductivity material converges to a shape different from the low conductivity one. An improved shape is obtained from the SG guess (sharp tip) than from the RG guess (blunt tip) for the highly conductive material. The sharp-tip cross-section for the unit-cell fin is well described by a parabolic profile, which has, in general, higher efficiency than triangular or rectangular profiles (see [18, p. 409]).

The importance of our result is in automatically generating optimal shape profiles for the fins as well as the spacing between the individual fins for maximized efficiency. We could do even better in terms of the spacing by having the outer limit of the boundary layer from one fin "just touch" the one from the adjacent fin. Our use of a function for describing the profile of the cross-section prevents us from reaching such a shape. We are currently investigating the use of a general curve instead of a function for approximating the profile of the fin.

Table 3
Optimization results with the additional constraint imposed on the slope of the design boundary at the ends of the periodic fin for the RG case

Material and number of iterations	Initial values of DVs (m)	Final values of DVs (m)	Initial value of heat flux (W/m^2)	Final value of heat flux (W/m^2)	Area constraint final value	Boundary layer constraint final value
Al	RG 0.042	0.015				
10 iterations	0.045	0.0275	993.1	1554.05	0.11	-0.45×10^{-3}
	0.050	0.0456				
Unit-conductivity	RG 0.042	0.015				
10 iterations	0.045	0.0278	802.6	1253.6	0.11	-0.55×10^{-3}
	0.050	0.0465				

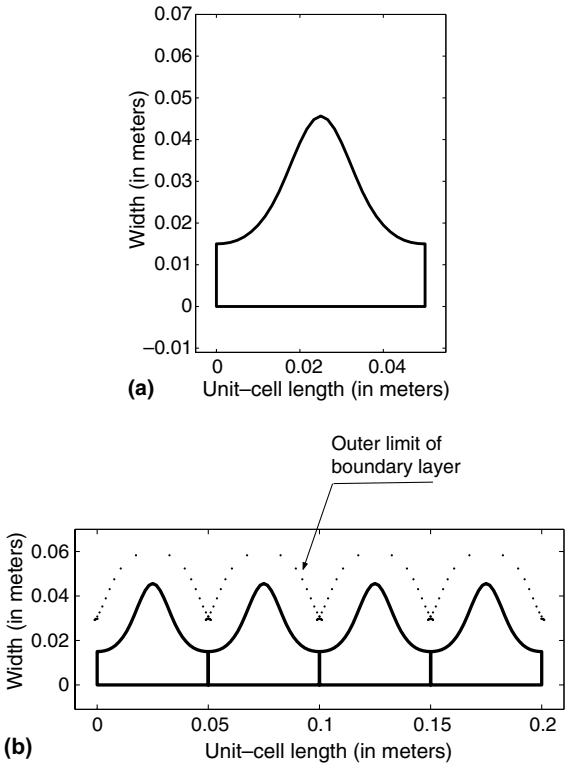

Fig. 7. Imposing the additional constraint of zero slope at the ends of the fins, we virtually eliminate the overlap of the boundary layer in the periodic array of fins. The objective function value in this case is the true amount of heat-flux passing through the fin. (a) Final shape of unit-cell for aluminum fin starting from the RG. A constraint of zero slope of the boundary at the ends of the fin is imposed. (b) The periodic array of aluminum fins for the RG initial shape. For highly conductive materials, this shape is less efficient than that in Fig. 6(b).

5. Conclusions and future work

In this paper we advanced a method for automatically determining the optimal shape and configuration or spacing between fins in a cooling fin array under natural convection conditions and we determined a connection between shape and conductivity parameters.

We employed the element-free Galerkin (EFG) method as the analysis method for solving the heat equations for every iteration of the shape optimization setup. The goal was to provide a scheme for *automatically* determining the optimal shape of a conduction–diffusion system and note the shape dependence on the conductivity parameters. We formulated a general framework based on a meshfree solution of the non-linear heat-transfer equations coupled with a gradient-based algorithm for constrained optimization to determine the characteristics of the optimal shapes for *varying conductivity parameters*. We solved the optimal shape problem in the context of laminar flow for natural convection. Other types of conditions can be considered using the current development.

We allowed flexibility in determining the best shape for the individual fins and we also automatically found the optimal spacing between them. We used a starting shape an unfinned shape with a rectangular cross-section and in few iterations obtain the fin shape. The array of fins was built using periodic boundary conditions. Highly conductive fins end up in sharp-pointed thin fins whereas low conductivity fins converge to thicker, rounded-tip fins. These results seem to correlate to the optimal shapes seen in natural systems that perform under similar conditions: intestinal villi in mass transfer (blunt tip and wide base) and stegosaurus plates (long and thin cross-section). This correlation suggests that intestinal villi have a low mass diffusivity (relative to their mass transfer coefficient) while stegosaurus fins have a large thermal conductivity (relative to their heat transfer coefficient).

In this work we used a one-dimensional directional change of the shape design variables. To implement a more general motion and transformation of the designable boundary we are currently investigating a meshfree solution in the context of the fictitious domain method. The high smoothness of the approximation functions in the meshfree approach can eliminate the difficulties faced by the FEM, which leads to non-differentiability of the objective function.

Acknowledgments

This work was partially supported through a Layman Fund award and a Fling Faculty Research Fellowship from the University of Nebraska-Lincoln, and by a NASA Nebraska Space Grant & EPSCoR award monitored by Dr. Brent Bowen and Ms. Mary Fink.

References

[1] D.Q. Kern, A.D. Kraus, Extended Surface Heat Transfer, McGraw-Hill, New York, 1972.
[2] A.D. Kraus, A. Bar-Cohen, Design and Analysis of Heat Sinks: Theory and Design, Wiley, 1995.
[3] S. Lee, Optimum design and selection of heat sinks, IEEE Trans. Comp., Packaging, Manufact. Technol., Part A 18 (1995) 812–817.
[4] R. Viswanath, V. Wakharkar, A. Watwe, V. Lebonheur, Thermal performance challenges from sillison to systems, Intel Technol. J. Q3 (2000) 1–15. http://www.intel.com/technology/itj.
[5] A. Bar-Cohen, Fin thickness for an optimized natural convection array of rectangular fins, J. Heat Transfer 101 (1979) 564–566.
[6] A. Bar-Cohen, W.M. Rohsenow, Thermally optimum spacing of vertical, naturally convection cooled, parallel plates, J. Heat Transfer 106 (1984) 116–123.

[7] A. Bejan, N. Dan, Constructal trees of convective fins, J. Heat Transfer 121 (1999) 675–682.
[8] M. Neagu, A. Bejan, Three-dimensional tree constructs of "constant" thermal resistance, J. Appl. Phys. 86 (12) (1999) 7107–7115.
[9] J.W. Hou, J.S. Sheen, C.H. Chuang, Shape-sensitivity analysis and design optimization of linear, thermoelastic solids, AIAA J. 30 (2) (1992) 528–537.
[10] E.J. Haug, K.K. Choi, V. Komkov, Design Sensitivity Analysis of Structural Systems, Academic Press, New York, 1986.
[11] J. Haslinger, R.A.E. Mäkinen, Introduction to Shape Optimization, SIAM, Philadelphia, 2003.
[12] T. Belytschko, Y. Krongauz, D. Organ, M. Fleming, P. Krysl, Meshless methods: An overview and recent developments, Comput. Meth. Appl. Mech. Eng. 139 (1996) 3–47.
[13] S. Li, W.K. Liu, Meshfree and particle methods and their applications, Appl. Mech. Rev. 55 (2002) 1–34.
[14] F. Bobaru, Meshless methods in shape optimization of linear elastic and thermoelastic solids, PhD thesis, Cornell University, Ithaca, NY, 2001.
[15] F. Bobaru, S. Mukherjee, Shape sensitivity analysis and shape optimization in planar elasticity using the element-free Galerkin method, Comput. Meth. Appl. Mech. Eng. 190 (32–33) (2001) 4319–4337.
[16] F. Bobaru, S. Mukherjee, Meshless approach to shape optimization of linear thermoelastic solids, Int. J. Numer. Meth. Eng. 53 (4) (2002) 765–796.
[17] F. Bobaru, S. Rachakonda, Boundary layer in shape optimization of convective fins using a meshfree approach, Int. J. Numer. Meth. Eng. 60 (7) (2004) 1215–1236.
[18] J.L. Plawsky, Transport Phenomena Fundamentals, Marcel Dekker, New York, 2001, pp. 410–412.
[19] J.O. Farlow, C.V. Thompson, D.E. Rosner, Plates of stegosaurus. Forced convection heat loss fins?, Science 192 (1976) 1123–1125.
[20] A. Bejan, From heat transfer principles to shape and structure in nature: constructal theory, J. Heat Transfer 122 (2000) 430–449.
[21] A. Bejan, Shape and Structure, from Engineering to Nature, Cambridge University Press, Cambridge, UK, 2000.
[22] T. Belytschko, Y.Y. Lu, L. Gu, Element-free Galerkin methods, Int. J. Numer. Meth. Eng. 37 (1994) 229–256.
[23] J. Hadamard, Le probleme the Cauchy, Hermann, Paris, 1932.
[24] A. Akima, A new method of interpolation and smooth curve fitting based on local procedures, J. Assoc. Comput. Mach. 17 (1970) 589–602.
[25] IMSL numerical libraries, Visual Numerics, Inc., http://www.vni.com.
[26] K. Schittkowski, NLPQL: a FORTRAN subroutine solving nonlinear programming problems, Ann. Oper. Res. 5 (1986) 485–500.
[27] J. Nocedal, S.J. Wright, Numerical Optimization, Springer-Verlag, New York, 1999.
[28] R.T. Haftka, Z. Gürdal, Elements of Structural Optimization: Third Revised and Expanded Edition, Kluwer Academic Publishers, 1992.
[29] F.M. White, Heat and Mass Transfer, Addison-Wesley, 1988.
[30] J.S. Chen, C. Pan, C.T. Wu, W.K. Liu, Reproducing kernel particle methods for large deformation analysis of non-linear structures, Comput. Meth. Appl. Mech. Eng. 139 (1996) 195–227.
[31] F. Bobaru, S. Rachakonda, An ill-posed problem in inverse optimal shape design of cooling fins and its regularization, in: Proceedings of the Second MIT Conference on Computational Fluid and Solid Mechanics, MIT campus, Cambridge, MA, USA, 17–20 June 2003.
[32] F. Bobaru, Stegosaurus plates, intestinal villi, and optimal shapes of cooling fins, submitted for publication.